JOURNAL OF ENERGY SYSTEMS

2022, 6(2)

2602-2052 DOI: 10.30521/jes.952627 Research Article

Numerical investigation of energy desorption from magnesium nickel hydride based thermal energy storage system

Sumeet Kumar Dubey
Indian Institute of Technology, Department of Energy Science and Engineering (formerly Centre for Energy Studies), Delhi, New Delhi, India-110016, dubeysumeet92@gmail.com
K. Ravi Kumar*
Indian Institute of Technology, Department of Energy Science and Engineering (formerly Centre for Energy Studies), Delhi, New Delhi, India-110016, krk@ces.iitd.ac.in

Submitted: 15.06.2021
Accepted: 19.03.2022
Published: 30.06.2022

* Corresponding Author

Abstract: The use of dual metal hydride system for thermal energy storage consists of high and low-temperature metal hydrides. In this study, a 3D cylindrical Magnesium Nickel hydride bed is analyzed for thermal energy discharge. The energy discharge from metal hydride bed initially at temperature of 400 K, a heat transfer fluid at 500 K temperature is supplied to extract the heat generated due to exothermic chemical reaction. In this article, variation of the number of heat transfer fluid tubes and effect of variation of aspect ratio (ratio of diameter to height) on energy desorption and heat transfer from metal hydride bed is performed. The optimal number of heat transfer fluid tubes is determined for various aspect ratios. The temperature variation of the metal hydride bed with an increase in the number of heat transfer fluid tubes is analyzed. The study of aspect ratio variation on energy desorption and heat transfer characteristics is analyzed for three aspect ratios 0.5, 1, and 2. The variation of thermal energy desorbed, net heat transfer and temperature variation of metal hydride bed are analyzed. The adequate number of heat transfer fluid tubes for AR 0.5, 1, and 2 is identified as 32, 48, and 72, respectively. The cumulative heat released from MH bed with AR 0.5, 1, and 2 is 350.94 kJ, 330.56 kJ, and 310.42 kJ, respectively. The study will be useful in designing the optimized metal hydride bed reactor for thermal energy storage applications.

Keywords: *Energy desorption, High temperature metal hydride, Magnesium Nickel metal hydride, Thermal energy storage*

Cite this paper as: Dubey, S. K., & Kumar, K, R., Numerical investigation of energy desorption from magnesium nickel hydride based thermal energy storage system. *Journal of Energy Systems* 2022; *6*(2): 165-175, DOI: 10.30521/jes.952627

Abbreviations	Descriptions
ACR	Area cross-section ratio
AR	Aspect ratio
HTF	Heat transfer fluid
HTMH	High temperature metal hydride
LTMH	Low temperature metal hydride
MH	Metal hydride
TCES	Thermochemical energy storage
TES	Thermal energy storage
Greek letter	**Descriptions**
Δh	Enthalpy of reaction (J/mol)
Δs	Entropy of reaction (J/mol K)
ε	Porosity
μ	Dynamic viscosity (Pa s)
ρ	Density (kg/m^3)
K	Permeability (m^2)
σ	Thermal conductivity (W/m K)
Nomenclature	**Description**
A	Constant {Δs/R}
B	Constant {Δh/R} (K)
C	Rate constant (1/s)
c	Specific heat capacity (J/kg K)
D	Diameter of MH bed (mm)
d	Diameter of HTF tubes (mm)
E	Activation energy (J/mol H_2)
l	Length of MH bed (mm)
M	Molar mass (g/mol)
p	Pressure (bar)
R	Universal gas constant (J/mol K)
r	Radius
T	Temperature (K)
t	Time (s)
Subscript	**Description**
a	Absorption
eff	Effective
eq	Equilibrium
h	Hydrogen
HTF	Heat transfer fluid
m	Mass
s	Metal hydride
sat	Saturation

1. INTRODUCTION

Several international agencies have reported a rapid increase in energy demand due to technological advancement and increase in population [1,2]. Due to the increase in energy demand, the burden on the conventional fuel reserves has led to increased pollution, global warming, and the extinction of conventional fuel reservoirs. The challenges mentioned above can be addressed by utilizing renewable energy sources. Among the renewable energy sources, solar energy has enormous potential to satisfy the rising energy need. The challenges in solar energy technologies are diurnal variation and intermittent nature results in poor dispatchability. This issue can be resolved by using thermal energy storage (TES) system. Integration of TES system with the solar thermal power generation and industrial process heat applications can help to overcome the challenges mentioned above.

Thermal energy storage is broadly categorized as sensible, latent, and thermochemical energy storage [3,4]. Sensible energy storage systems store heat by increasing the temperature of working media, while latent energy storage systems store heat by changing the phase of the working media [5]. The thermochemical energy storage (TCES) stores/releases energy by undergoing chemical reactions. The endothermic reaction stores thermal energy, while exothermic chemical reaction discharges the stored energy. TES using metal hydride (MH) is one of the well-known TCES techniques. The MH-based TCES technique has good reversibility, cyclic stability, wide range of temperature flexibility, and higher gravimetric and volumetric energy storage density.

The dual bed MH-based TES system is represented in Fig. 1. The thermal energy collected in solar field and transported to high temperature metal hydride (HTMH) using heat transfer media. The endothermic reaction takes place in HTMH, which is represented blue color dashed line. The hydrogen is liberated from HTMH and supplied to low-temperature metal hydride (LTMH). Due to hydrogen absorption in LTMH, an exothermic reaction occurs, and heat (Q_r) is generated at low temperature. When the heat stored in HTMH is required to be released, hydrogen stored in LTMH is supplied to HTMH, represented by red color dashed with a double dot line. In a dual MH-based TES system, HTMH acts as thermal energy storage media while LTMH acts as hydrogen storage media.

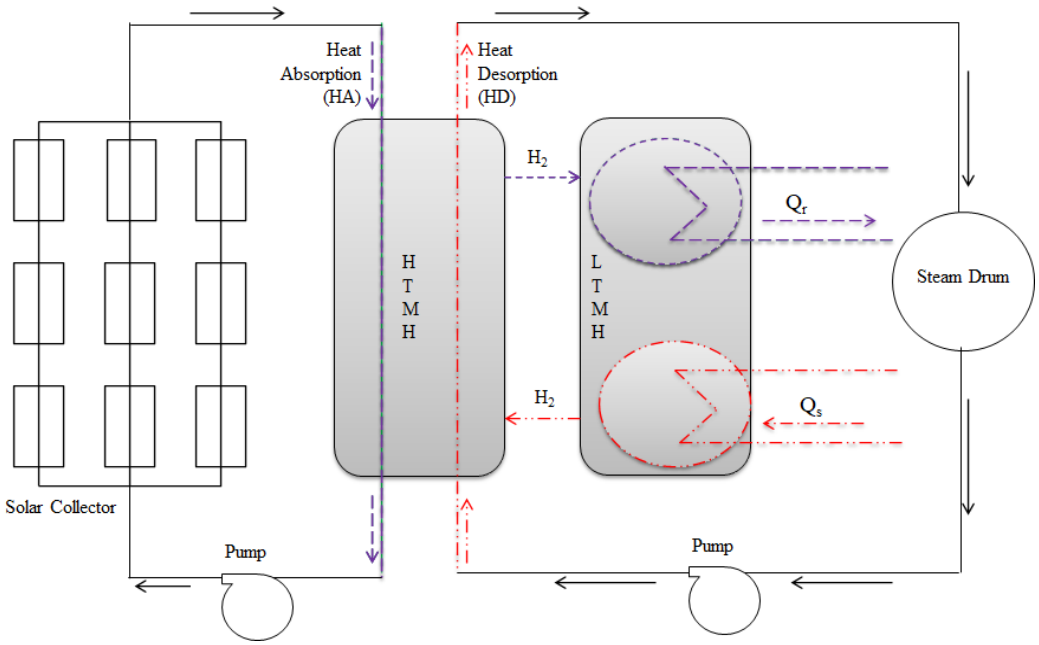

Figure 1. Schematic of dual MH based TCES system [3].

Magnesium (Mg) based MH attracted researchers for TES due to its high energy density and lower cost. In earlier studies, Mg-based MH was developed with different capacities to analyze its feasibility for various applications [5,6,7]. Many numerical analyses have been performed on coupled HTMH and LTMH TES system. Mg_2FeH_6 as HTMH and Na_3AlH_6 as LTMH were studied for the feasibility of a dual MH-based TES system [8]. The study reported 132 kWh/m^3 energy storage density with the operating temperature range of 450-500 ºC. Similar MH (Mg_2FeH_6 and Na_3AlH_6) pairs were studied with fins to enhance heat transfer from the MH reactor [9], and reported 90 kWh/m^3 energy storage density with 96% storage efficiency. A similar type of study with $NaMgH_2F$ and $TiCr_{1.6}Mn_{0.2}$ as HTMH and LTMH, respectively, was performed for dual MH-based TES system feasibility [10]. The study concluded 226 kWh/m^3 energy storage density with a higher operating temperature at 600 ºC. In another study, Mg_2Ni and $LaNi_5$ was used as HTMH and LTMH. The system reported a storage efficiency and energy storage density as 89.4% and 156 kWh/m^3 respectively [11]. Pair of $LaNi_{4.25}Al_{0.75}$ and $LaNi_5$ is also analyzed for thermal energy storage at 150 ºC [12]. Energy storage density and energy storage efficiency of the dual metal hydride bed system was reported as 111 kWh/m^3 and 91% respectively. Several other studies [13,14,15,16,17] performed on MH reported the use of MH as a potential technique for TES. An extensive analysis of heat transfer from individual MH bed necessary to evaluate dual MH bed system's performance. The effective heat transfer is responsible for higher hydrogen absorption which is directly affecting the net energy desorption from the MH bed. Extensive studies have been performed on the MH bed to enhance heat transfer by using fins, and improved heat exchanger design and different reactor geometry. The novelty of the study includes the study of effect of geometric parameter variation and the number of heat transfer fluid (HTF) tubes on the heat transfer and energy discharge characteristics has been discussed in this study.

This study includes the analysis of energy discharge from Magnesium Nickel-based MH using COMSOL Multiphysics 5.5. The study includes study of the number of HTF tubes and aspect ratio (AR) on energy desorption and heat transfer from MH bed. The adequate number of HTF tubes is determined by considering the variation of MH bed temperature with number of HTF tubes and parameter area cross section ratio (ACR). The variation of thermal energy desorbed, net heat transferred and temperature variation across the MH bed is analyzed for various geometrical parameters. Based on the analysis of aspect ratio variation, the geometry with effective heat transfer and heat desorption is determined. The novelty of the study includes the variation of geometric parameter (aspect ratio) for a 3-D geometry along with the parameter "area cross section ratio" introduced for determining the effective number of HTF tubes. This study will be helpful in developing a metal hydride TES system with effective heat transfer.

2. MODELING OF THERMAL ENERGY STORAGE SYSTEM

2.1. Computational Domain

Magnesium nickel hydride of 1 kg is packed in cylindrical geometry, taking porosity as 0.5. Since the cylindrical MH bed is symmetric to the x and y axis, one-fourth of the geometry is considered for the energy desorption analysis. The three-aspect ratio (AR) configurations having a different number of HTF tubes are shown in Fig. 2. Aspect ratio is expressed as the ratio of diameter (D) to height (H) of MH bed.

$$AR = \frac{Diameter\ of\ metal\ hydride\ bed}{Length\ of\ metal\ hydride\ bed} \quad (1)$$

Another parameter area cross section ratio (ACR) is used to determine the number of HTF tubes for aspect ratio 0.5 and 2 which is defined as:

$$ACR = \frac{Cross-sectional\ area\ of\ MH\ bed}{Cross-sectional\ area\ of\ all\ the\ tubes} = \frac{\left(\frac{\pi D^2}{4}\right)}{\left(n * \frac{\pi d^2}{4}\right)} = \frac{D^2}{n * d^2} \quad (2)$$

In the cylindrical MH, a single circle at the center represents the hydrogen supply tube. The concentric circles represent the axial HTF tubes distributed radially in the MH bed cross-section. The dimensions of the geometry and HTF tubes considered in the geometry are listed in Table 1.

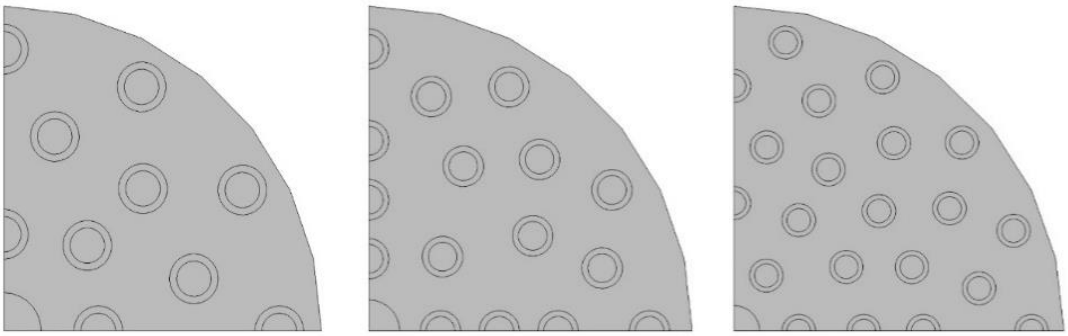

a) *b)* *c)*

Figure 2. Computational domain for aspect ratio a) 0.5, b) 1, and c) 2.

Table 1. Dimensions of MH bed considered for analysis.

Dimension	AR 0.5	AR 1	AR 2
Diameter of MH bed (mm)	80.7	99.1	122
Diameter of hydrogen supply tube (mm)	9.5	9.5	9.5
Outer diameter of HTF tubes (mm)	6.4	6.4	6.4
Inner diameter of HTF tubes (mm)	4.4	4.4	4.4
Height of MH bed and tubes (mm)	161.4	99.1	61
Number of tubes	32	48	72

2.2. Assumptions

-Hydrogen is assumed as ideal gas.
-Hydrogen gas and MH bed are in thermal equilibrium.
-Metal hydride material is homogenous and isotropic.
-Effect of radiation is not considered in the analysis.
-Thermal properties of MH, hydrogen, and HTF, such as thermal conductivity, specific heat capacity, etc., remain constant throughout the process.

2.3. Governing Equations

This section includes the governing equations of mass, momentum, and energy conservation used in the analysis.

Mass conservation equation:

The continuity equation for MH bed, hydrogen gas, and HTF are given as [12]:

$$\varepsilon \frac{\partial \rho_h}{\partial t} + \nabla.(\rho_h u_h) = -S_m \quad (3)$$

$$(1-\varepsilon)\frac{\partial \rho_s}{\partial t} = S_m \quad (4)$$

Eqs. 3 and 4 represent the mass balance equation for hydrogen in pores and MH bed, respectively. S_m is the rate of mass of hydrogen absorbed per unit volume. The negative sign indicates the reduction in the mass of hydrogen. The positive sign indicates the absorption of hydrogen in MH.

$$S_m = C_a exp\left(\frac{-E_a}{RT}\right) ln\left(\frac{p}{p_{eq}}\right)(\rho_{s\,sat} - \rho_s) \quad (5)$$

$$ln\left(\frac{p}{p_{eq}}\right) = A - \frac{B}{T} \quad (6)$$

Eq. 5 determines the mass of hydrogen absorbed per unit volume and Eq. 6 is a well-known van't Hoff equation. C_a and E_a are rate constant and activation for hydrogen absorption in MH. p and p_{eq} are supply pressure of Hydrogen and equilibrium pressure of MH bed. $\rho_{(s\,sat)}$ is the saturation density of MH.

$$\frac{\partial \rho_h}{\partial t} + \nabla.(\rho_h u_h) = 0 \quad (7)$$

$$\frac{\partial \rho_{HTF}}{\partial t} + \nabla.(\rho_{HTF} u_{HTF}) = 0 \quad (8)$$

Here, ρ is the density, ε is the porosity of MH bed. Equations (7) and (8) represent the mass balance equation for hydrogen in supply tube and HTF, respectively.

Momentum conservation equation:

Navier-Stokes equation is used for free-flowing hydrogen and HTF, while the Brinkman equation is used for hydrogen flow in porous media as in Ref. [9]:

$$\frac{\rho_h}{\varepsilon}\left(\frac{\partial u_h}{\partial t} + u_h.\frac{\nabla u_h}{\varepsilon}\right) = -\nabla p + \nabla.\left[\frac{\mu_h}{\varepsilon}(\nabla u_h + (\nabla u_h)^T) - \frac{2}{3}\frac{\mu_h}{\varepsilon}(\nabla.u_h)\right] - \frac{\mu_h}{K}u_h + \frac{S_m}{\varepsilon^2}u_h \quad (9)$$

$$\rho_h\left(\frac{\partial u_h}{\partial t} + u_h.\nabla u_h\right) = -\nabla p + \nabla.\left[\mu_h(\nabla u_h + (\nabla u_h)^T) - \frac{2}{3}\mu_h(\nabla.u_h)\right] \quad (10)$$

$$\rho_{HTF}\left(\frac{\partial u_{HTF}}{\partial t} + u_{HTF}.\nabla u_{HTF}\right) = -\nabla p + \nabla.\left[\mu_{HTF}(\nabla u_{HTF} + (\nabla u_{HTF})^T) - \frac{2}{3}\mu_{HTF}(\nabla.u_{HTF})\right] \quad (11)$$

Here, u is the velocity, μ is dynamic viscosity of Hydrogen gas and K is permeability of porous MH bed. Eq. 9 is the Brinkman equation for hydrogen flow in porous domain and Eqs. 10 and 11 represent the Navier-Stokes equation for hydrogen flow in supply tube and HTF.

Energy conservation equation:

As discussed in the assumption, thermal equilibrium exists between MH and hydrogen gas flowing in porous structure:

$$(\rho c_p)_{eff}\frac{\partial T}{\partial t} + \rho c_{ph}(u_h.\nabla T) = \nabla.(\sigma_{eff}\nabla T) + S_T \quad (12)$$

$$(\rho c_p)_{eff} = \varepsilon(\rho c_p)_h + (1-\varepsilon)(\rho c_p)_s \quad (13)$$

$$\sigma_{eff} = \varepsilon\sigma_h + (1-\varepsilon)\sigma_s \quad (14)$$

$$S_T = S_m(\Delta h) \quad (15)$$

$$(\rho_h c_{ph})\left(\frac{\partial T}{\partial t} + u_h.\nabla T\right) = \nabla.(\sigma_h \nabla T) \quad (16)$$

$$(\rho_{HTF} c_{pHTF})\left(\frac{\partial T}{\partial t} + u_{HTF}.\nabla T\right) = \nabla.(\sigma_{HTF}\nabla T) \quad (17)$$

Here, c_p is the specific heat capacity and σ is the thermal conductivity. Eqs. 12,16 and 17 are the energy balance equations for MH, hydrogen flow in supply tube, and HTF, respectively. The thermochemical properties of the MH, hydrogen, and HTF used in the analysis are listed in Table 2.

Table 2. Thermodynamic and chemical properties of a MH, hydrogen, and HTF [18-21].

Properties	Value
Energy desorption rate constant (1/s)	175.1
Activation energy for energy desorption (J/mol)	52205
Reaction enthalpy (J/mol)	64230
Reaction entropy (J/mol K)	124.3
Universal gas constant (J/mol K)	8.314
Specific heat capacity of HTF (J/kg K)	2101
Molecular weight of HTF (g/mol)	166
Thermal conductivity of HTF (W/m K)	0.11
Dynamic viscosity of HTF (Pa.s)	0.345
Density of HTF (kg/m^3)	895
Porosity of MH bed	0.5
Permeability of MH bed (m^2)	10.Ağu
Specific heat capacity of MH (J/kg K)	1414
Density of unsaturated MH (kg/m^3)	3200
Density of saturated MH (kg/m^3)	3319.3
Thermal conductivity of MH (W/m K)	0.2
Thermal conductivity of hydrogen (W/m K)	0.1815
Molecular weight of hydrogen (g/mol)	2.Oca
Specific heat capacity of hydrogen (J/kg K)	14890
Density of hydrogen (kg/m^3)	0.0838
Dynamic viscosity of hydrogen (Pa.s)	$9.0510^{-6} \times (T/293)^{0.68}$

2.4. Initial Values and Boundary Conditions

The initial values at t = 0 for MH bed, Hydrogen in supply tube, HTF, and Copper tube, are listed in Table 3.

Table 3. Initial conditions of different domains.

Parameters	MH bed	Hydrogen in supply tube	Heat transfer fluid
Temperature (T_{ini})	500 K	298 K	500 K
Pressure (p_{ini})	1 bar	1 bar	1 bar

The initial pressure of the MH bed is the equilibrium pressure corresponding to the initial temperature of the MH bed. The initial temperature of the copper tubes is taken the same as the HTF temperature. The unsaturated MH bed density is $\rho_{ini,s}$ = 3200 kg/m^3. The top, bottom, and outermost surface of the MH bed are insulated, while the top and bottom edge of the copper tube is insulated.

$$\left|\frac{\partial T}{\partial r}\right|_{r=r_o} = 0 \quad \left|\frac{\partial T}{\partial r}\right|_{l=l_b} = 0 \quad \left|\frac{\partial T}{\partial r}\right|_{l=l_t} = 0$$

2.5. Model Validation

The model is validated with experimental study Jemni et al [23]. It has a cylindrical MH bed with a hydrogen supply at the top center of the cylinder. The reactor is kept in a constant temperature thermal bath to extract heat generated during hydrogen absorption. The temperature at a point in the MH bed is plotted with time. The temperature of the MH bed has a maximum absolute error of less than 2% with the Jemni et al [23], as shown in Fig. 3. The basic physics used in the present model is same as used in the validated model. The variation in the results may be due to the assumptions considered in the numerical analysis such as homogenous and isotropic metal hydride and the constant thermophysical properties, which may not be constant in the experimental study performed by Jemni et al [23].

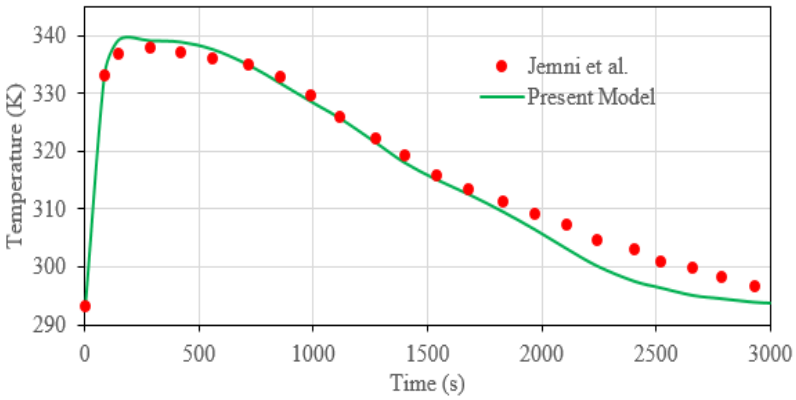

Figure 3. Validation of the present model with the Jemni et al [23].

2.6. Grid Independent Study

The mesh elements are increased gradually to study the average MH bed temperature variation. The variation of the number of mesh elements from 22914 to 28100 shows almost no variation in average MH bed temperature as shown in Fig. 4. Thus, 22914 elements are considered suitable for analysis.

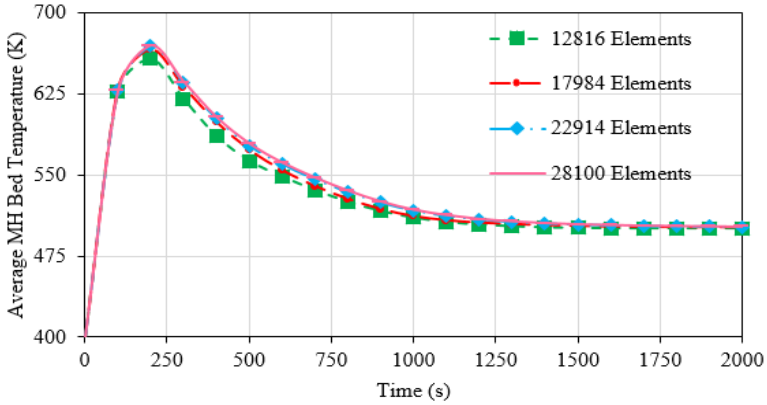

Figure 4. Grid independent study of the computational domain.

3. RESULTS AND DISCUSION

The results discussed in this study are divided into two parts: a) Variation of the number of heat transfer fluid tubes b) Effect of variation of aspect ratio on energy desorption characteristics of Magnesium Nickel MH.

3.1 Variation of Number of Heat Transfer Fluid Tubes

Variation in the number of HTF tubes, geometry with AR 1 is considered for the analysis. The number of HTF tubes for AR 1 is increased from 36 to 54 tubes. The variation of average MH bed temperature is studied and is shown in Fig. 5. The MH bed's temperature seems to decrease significantly when the number of HTF tubes increased from 36 to 48, but a further increase in the number of HTF tubes from 48 to 54 has no significant change in MH bed temperature. Similar results are also observed when the MH bed temperature is plotted with time, as shown in Fig. 6. The number of HTF tubes play a major role in removal of heat from the MH bed, which is indicated by the MH bed temperature; therefore, the average temperature of the MH bed has been considered to study the various geometrical parameters of the MH bed. Increasing the number of HTF tubes increase the system's cost without any significant change in MH bed temperature. Therefore, 48 number of HTF tubes are decided as adequate for the case of AR 1.

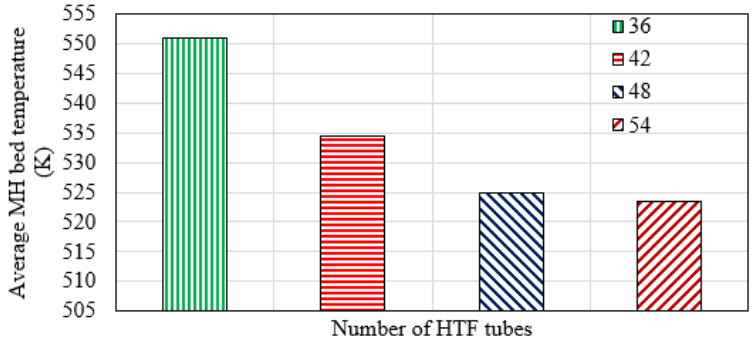

Figure 5. Variation of average MH bed temperature with different HTF tubes

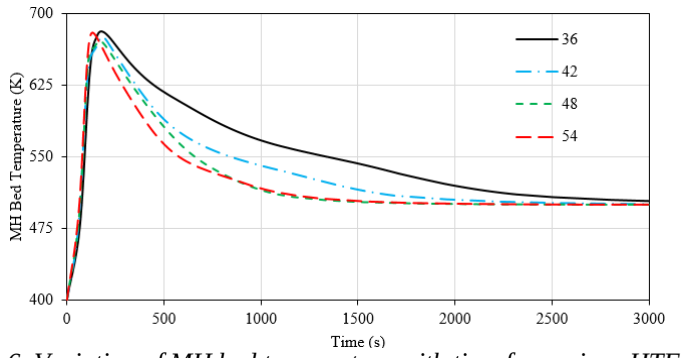

Figure 6. Variation of MH bed temperature with time for various HTF tubes.

The number of HTF tubes for AR 0.5 and 2 is calculated using the term area cross-section ratio (ACR) defined in Eq. 2. The term ACR represents the number of HTF tubes per unit volume of MH bed.

The value of ACR calculated for AR 1 is 5.298. The same value is considered for AR 0.5 and 2 to calculate the number of HTF tubes. Based on the ACR, the number of HTF tubes calculated for AR 0.5 and 2 is 32 and 72, respectively.

3.2. Variation of Aspect Ratio

The adequate number of HTF tubes for the aspect ratio 0.5, 1, and 2 is 32, 48, and 72, respectively. This section discussed the effect of variation of aspect ratio on temperature and energy desorption characteristics. The amount of cumulative heat released and net heat transfer from the MH bed is represented in Figs. 7 and 8, respectively. The cumulative heat represents the total thermal heat released due to an exothermic chemical reaction between metal alloy and hydrogen, while the net heat transfer represents the fraction of cumulative heat which is taken away by the HTF. The cumulative heat released and net heat transfer from the MH bed is observed maximum for AR 0.5. The amount of cumulative heat released for aspect ratios 0.5, 1, and 2 are 350.94 kJ, 330.56 kJ, and 310.42 kJ, respectively. The net heat transfer from the MH bed for aspect ratios 0.5, 1, and 2 are 288.31 kJ, 269.04 kJ, and 253.12 kJ, respectively. The heat transfer in radial direction is significantly higher than in the axial direction at a lower aspect ratio. With the increase in aspect ratio, the radial dimension of the MH bed increases. The increase in radial dimension increases the radial heat resistance, which reduces heat transfer from the MH bed when the aspect ratio is increased. The temperature variation of cross-section of MH bed at various axial lengths with time is represented in Fig. 9. The temperature contours of the cross-section of the MH bed give a comparison of temperature variation with aspect ratio. Temperature contours represents that the temperature of the MH bed is lower and more uniform for the lower aspect ratio as shown in Fig. 9. The steady-state of the MH bed is achieved faster in a lower aspect ratio. Based on the analysis, it is clear that the MH bed with an aspect ratio of 0.5 is more suitable for energy desorption and effective heat transfer.

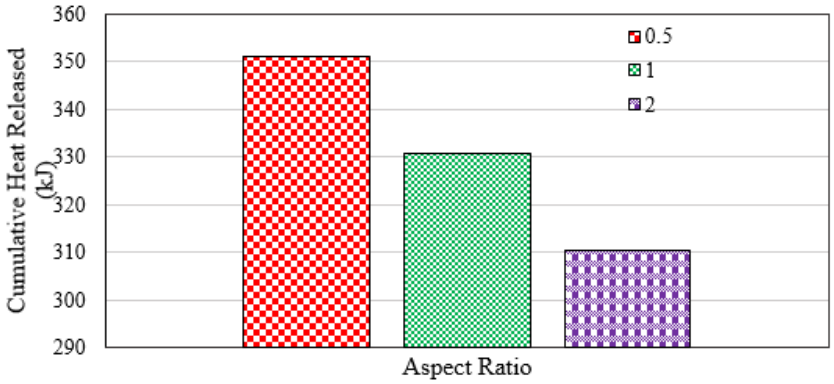

Figure 7. Cumulative heat released from the MH bed with aspect ratio

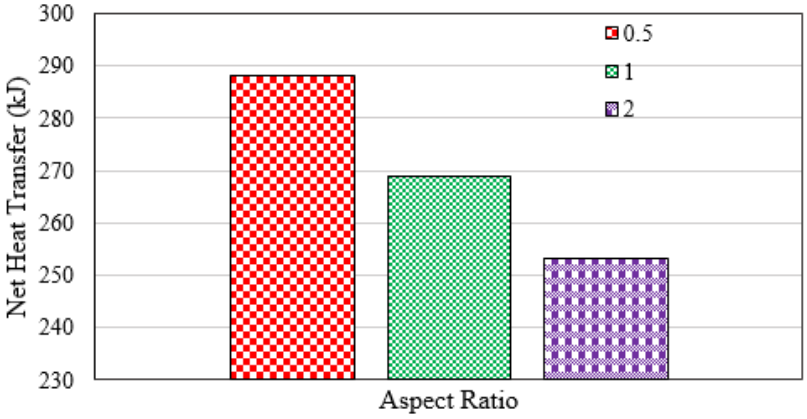

Figure 8. Net heat transfer from the MH bed with aspect ratio

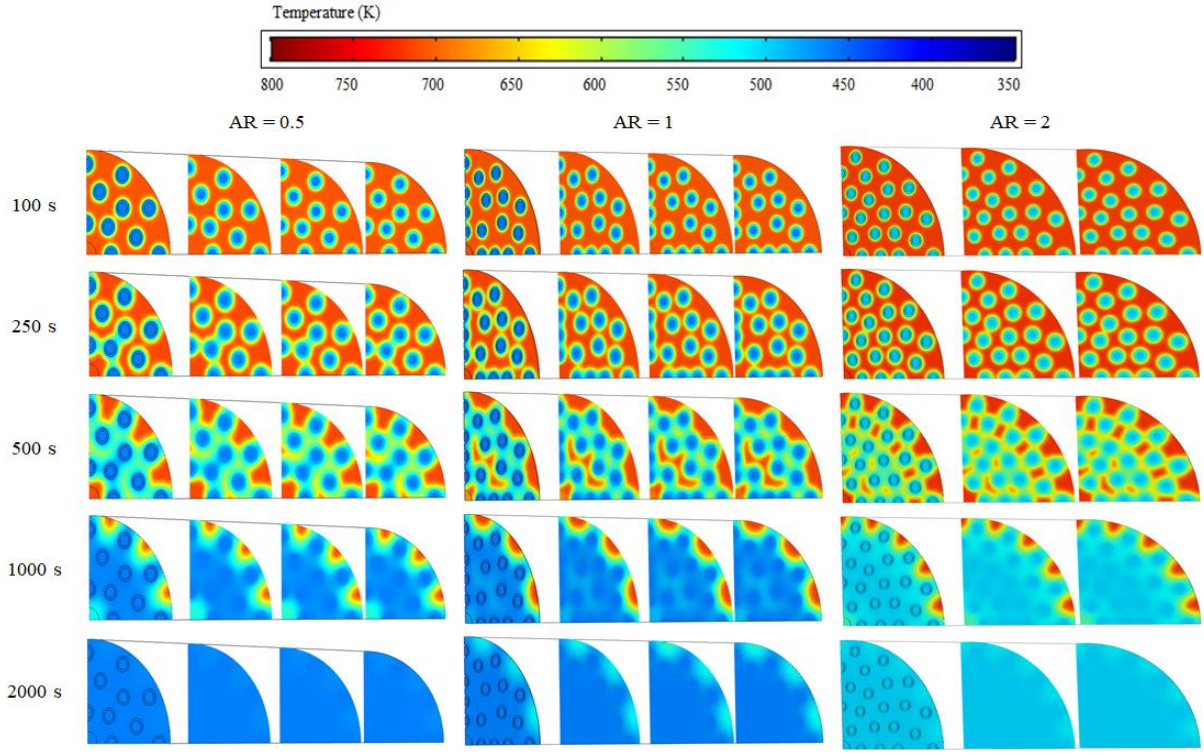

Figure 9. Temperature contours of MH bed with time for different aspect ratios

4. CONCLUSION

Magnesium Nickel MH is studied for thermal energy desorption and effective heat transfer from MH bed. The variation of number of HTF tubes has been studied for three different aspect ratios as 0.5, 1, and 2. The variation of MH bed temperature is studied to determine the adequate number of HTF for three aspect ratios. The variation of heat released and net heat transferred from the MH bed is also studied. The following observations are made based on the modeling results of 1 kg of Magnesium Nickel MH.

-The adequate number of HTF tubes for AR 0.5, 1, and 2 is 32, 48, and 72, respectively.
-Cumulative heat released from MH bed with AR 0.5, 1, and 2 is 350.94 kJ, 330.56 kJ, and 310.42 kJ, respectively.
-Net heat transfer from MH bed with AR 0.5, 1, and 2 is 288.31 kJ, 269.04 kJ, and 253.12 kJ, respectively.
-The average temperature of MH bed decreases due to effective heat transfer in lower aspect ratio geometries.
-The heat transfer from the MH bed increases with the lower radial dimension and higher axial dimensions.
-The study will be useful in designing the optimized MH bed reactor based thermal energy storage for industrial and power generation applications.

Acknowledgements

The authors are grateful to Indian Oil Corporation Limited, R & D Centre and Science and Engineering Research Board (SERB), Department of Science and Technology (DST), Government of India for providing the "Prime Minister Fellowship for Doctoral Research" to Mr. Sumeet Kumar Dubey through kind support from Confederation of Indian Industry (CII).

REFERENCES

[1] Cozzi, L, Gould, T, Bouckart, S, Crow, D, Kim, TY, McGlade, C, Olejarnik, P, Wanner, B, Wetzel, D. World Energy Outlook 2020. *IEA* 2020; *2050*(October): 1–461.
[2] IEA. India 2020 Policy Energy Review, 2017.
[3] Jain, S, Dubey, SK, Kumar, KR, Rakshit, D. Thermal Energy Storage for Solar Energy., In: Singh SN, Tiwari P, Tiwari S, editors. Fundamentals and Innovations in Solar Energy. Singapore : Springer, 2021, pp. 167–215. DOI: 10.1007/978-981-33-6456-1_9.
[4] Kumar, KR, Dashora, K, Krishnan, N, Sanyal, S, Chandra, H, Dharmaraja, S, Kumari, V. Feasibility assessment of renewable energy resources for tea plantation and industry in India-A review. *Renewable and Sustainable Energy Reviews* 2021; *145*: 111083.
[5] Jain, S, Kumar, KR, Rakshit, D. Heat transfer augmentation in single and multiple (cascade) phase change materials based thermal energy storage: Research progress, challenges, and recommendations. *Sustainable Energy Technologies and Assessments* 2021; *48*: 101633.
[6] Bogdanović, B, Spliethoff, B, Ritter, A. The magnesium hydride system for heat storage and cooling. *Zeitschrift für Physikalische Chemie* 1989;*164*(2):1497-1508. DOI: 10.1524/zpch.1989.164.Part_2.1497.
[7] Bogdanović, B, Ritter, A, Spliethoff, B, Straβburger, K. A process steam generator based on the high temperature magnesium hydride/magnesium heat storage system. *International journal of hydrogen energy* 1995; *20*(10): 811-822. DOI: 10.1016/0360-3199(95)00012-3.
[8] Paskevicius, M, Sheppard, DA, Williamson, K, Buckley, CE. Metal hydride thermal heat storage prototype for concentrating solar thermal power. *Energy* 2015; *88*: 469-477. DOI: 10.1016/j.energy.2015.05.068.
[9] d'Entremont, A, Corgnale, C, Sulic, M, Hardy, B, Zidan, R, Motyka, T. Modeling of a thermal energy storage system based on coupled metal hydrides (magnesium iron–sodium alanate) for concentrating solar power plants. *International Journal of Hydrogen Energy* 2017; *42*(35):22518-22529. DOI: 10.1016/j.ijhydene.2017.04.231.

[10] Mellouli, S, Askri, F, Edacherian, A, Alqahtani, T, Algarni, S, Abdelmajid, J, Phelan, P. Performance analysis of a thermal energy storage system based on paired metal hydrides for concentrating solar power plants. *Applied Thermal Engineering* 2018; *144*:1017-1029. DOI: .1037//0033-2909.I26.1.78.

[11] d'Entremont, A, Corgnale, C, Hardy, B, Zidan, R. Simulation of high temperature thermal energy storage system based on coupled metal hydrides for solar driven steam power plants. *International Journal of Hydrogen Energy* 2018; *43*(2): 817-830. DOI: 10.1016/j.ijhydene.2017.11.100.

[12] Malleswararao, K, Aswin, N, Murthy, SS, Dutta, P. Performance prediction of a coupled metal hydride based thermal energy storage system. *International Journal of Hydrogen Energy* 2020; *45*(32):16239-16253. DOI: 10.1016/j.ijhydene.2020.03.251.

[13] Malleswararao, K, Aswin, N, Murthy, SS, Dutta, P. Studies on a dynamically coupled multifunctional metal hydride thermal battery. *Journal of Alloys and Compounds* 2021; *866*: 158979.

[14] Tortoza, MS, Humphries, TD, Sheppard, DA, Paskevicius, M, Rowles, MR, Sofianos, MV, Aguey-Zinsou, KF, Buckley, CE. Thermodynamics and performance of the Mg–H–F system for thermochemical energy storage applications. *Physical Chemistry Chemical Physics* 2018; *20*(4): 2274-2283. DOI: 10.1039/c7cp07433f.

[15] Sheppard, DA, Paskevicius, M, Humphries, TD, Felderhoff, M, Capurso, G, von Colbe, JB, Dornheim, M, Klassen, T, Ward, PA, Teprovich, JA, Corgnale, C. Metal hydrides for concentrating solar thermal power energy storage. *Applied Physics A* 2016; *122*(395): 1-15. DOI: 10.1007/s00339-016-9825-0.

[16] Harries, DN, Paskevicius, M, Sheppard, DA, Price, TE, Buckley, CE. Concentrating solar thermal heat storage using metal hydrides. *Proceedings of the IEEE* 2011; *100*(2): 539-549. DOI:10.1109/JPROC.2011.2158509.

[17] Prasad, JS, Muthukumar, P, Desai, F, Basu, DN, Rahman, MM. A critical review of high-temperature reversible thermochemical energy storage systems. *Applied Energy* 2019; *254*:113733. DOI: 10.1016/j.apenergy.2019.113733.

[18] Kumar, KR, Chaitanya, NK, Kumar, NS. Solar thermal energy technologies and its applications for process heating and power generation–A review. *Journal of Cleaner Production* 2020; *282* :125296. DOI: 10.1016/j.jclepro.2020.125296.

[19] Chung, CA, Lin, CS. Prediction of hydrogen desorption performance of Mg2Ni hydride reactors. *International Journal of Hydrogen Energy* 2009; *34*(23): 9409-9423. DOI: 10.1016/j.ijhydene.2009.09.061.

[20] Mâad, HB, Askri, F, Virgone, J, Nasrallah, SB. Numerical study of high temperature metal-hydrogen reactor (Mg2Ni-H2) with heat reaction recovery using phase-change material during desorption. *Applied Thermal Engineering* 2018; *140*: 225-234. DOI: 10.1016/j.applthermaleng.2018.05.009.

[21] Malan, A, Kumar KR. Coupled optical and thermal analysis of large aperture parabolic trough solar collector. *International Journal of Energy Research* 2021; *45*(3): 4630-4651. DOI: doi.org/10.1002/er.6128

[22] Chung, C, Ho, CJ. Thermal–fluid behavior of the hydriding and dehydriding processes in a metal hydride hydrogen storage canister. *International Journal of Hydrogen Energy* 2009; *34*(10): 4351-4364. DOI: 10.1016/j.ijhydene.2009.03.028.

[23] Jemni, A, Nasrallah, SB, Lamloumi, J. Experimental and theoretical study of ametal–hydrogen reactor. *International Journal of Hydrogen Energy* 1999; *24*(7): 631-644. DOI: 10.1016/S0360-3199(98)00117-7.